

## Dependence of excess vibrational entropies on grain boundary structures in MgO: A first-principles lattice dynamics

T. Yokoi<sup>1,\*</sup>, Y. Arakawa,<sup>1</sup> K. Ikawa,<sup>1</sup> A. Nakamura<sup>1</sup> and K. Matsunaga<sup>1,2</sup>

<sup>1</sup>*Department of Materials Physics, Nagoya University, Nagoya 464-8603, Japan*

<sup>2</sup>*Nanostructures Research Laboratory, Japan Fine Ceramics Center, Nagoya 456-8587, Japan*



(Received 22 August 2019; accepted 24 January 2020; published 11 February 2020)

First-principles lattice dynamics calculations were performed to reveal an atomic-level origin of excess vibrational entropies at grain boundaries (GBs) in MgO. Fourteen symmetric tilt GBs with various structural units were systematically examined. The excess vibrational entropies were found to vary depending on the individual GBs, and as a result, the relative thermodynamic stability of the GBs studied changed with temperature. The excess GB volumes were less correlated with the excess vibrational entropies. By contrast, classifying ions in terms of their coordination numbers, bond-length changes at GBs were well correlated with atom-projected excess vibrational entropies for both Mg and O ions. Bond-length changes at GBs, which originate from changes in bond strength, are therefore a critical, well-defined descriptor for evaluating excess vibrational entropies and thereby excess free energies in MgO.

DOI: [10.1103/PhysRevMaterials.4.026002](https://doi.org/10.1103/PhysRevMaterials.4.026002)

### I. INTRODUCTION

In polycrystalline materials, grain boundary (GB) energies have critical impacts on their microstructure evolution and macroscopic properties, by governing grain-growth kinetics, impurity segregation, and precipitate nucleation. GBs with high GB energies were indicated to dominate GB sliding, leading to deformation and fracture in polycrystals [1,2]. Thermal grooving measurements in metals and oxides showed that GB energies decreased with rising temperature [3–5] while increased with increasing temperature for impurity-doped samples [6,7]. Such temperature dependence was also indicated to be closely related to abnormal and antithermal grain growth [6,8]. Understanding what determines GB energies at finite temperature is therefore essential for designing polycrystalline microstructures and the resulting material properties over a wide temperature range, as well as for developing GB physics.

In an earlier work by Readey and Jech, thermal grooving measurements for a tilt GB in NiO showed a strong reduction in GB energy with rising temperature. The authors attributed this reduction to GB segregation of Ni point defects [3]. Dillon *et al.* [6] and Kelly *et al.* [7] measured relative GB energies of impurity-doped Al<sub>2</sub>O<sub>3</sub> by measuring dihedral angles of thermal grooves at several temperatures. Their results showed that relative energies of the doped samples varied with temperature, suggesting that segregation/desegregation of impurities and complexion transition dominantly affect GB energies at finite temperatures.

However, the contribution of excess entropy to GB free energy is still not fully understood. A fundamental question is why excess entropies generated by GBs always have positive

values, as previous thermal grooving measurements indicated a reduction of relative GB free energies with temperature even for high-purity samples [6,7]. So far experimental measurement of excess entropies is difficult because their contribution to GB free energies cannot be separated from point defect formation and impurity segregation, whose concentrations significantly vary with temperature, for real polycrystals. It is also technically impossible to distinguish GB free energies from surface free energies, since measured dihedral angles provide only their ratio. Additionally, excess entropies are most likely to depend on GB structures as well as the chemical bonding states of substances, but such dependence is difficult to experimentally evaluate in the atomic and electronic levels. Therefore it is still unclear if and how excess entropies generated by GBs affect GB free energies at finite temperature.

Among many theoretical studies on the calculation of GB energies [9–17], a few studies with empirical interatomic potentials examined excess vibration entropies at GBs [13–17]. Using the harmonic approximation, Hashimoto *et al.* showed that an Al tilt GB with a specific structural unit had a larger excess entropy than the one without such a structural unit, speculating that this difference resulted from particular atoms next to the excess space of the GB [13]. Najafabadi *et al.* calculated excess vibrational entropies of stable and metastable structures for 12 twist GBs in Au [14]. Their study indicated a rough correlation between the excess free energies and excess volumes, although the reason was not discussed in detail. Harris *et al.* applied the quasiharmonic approximation to symmetric tilt GBs in MgO and indicated that the excess entropies had less effect on the excess free energies than the *PV* term with high pressures of up to 40 GPa [16]. To our knowledge, however, there are no studies that have revealed the atomic-level origin of excess vibrational entropies and also their dependence on chemical bonding states. A critical problem is that empirical interatomic potentials sometimes

\*Corresponding author: yokoi@mp.pse.nagoya-u.ac.jp

TABLE I. Crystallographic parameters of 14 symmetric tilt GBs.

Misorientation angle $2\theta$ (deg)	GB plane/ Rotational axis	$\Sigma$ value	$N_{\text{supercell}}$	Distance between GB planes (Å)
16.26	(710)/[001]	25	200	16.1
22.62	(510)/[001]	13	156	17.5
36.87	(310)/[001]	5	80	14.7
43.60	(520)/[001]	29	232	12.6
53.13	(210)/[001]	5	160	19.9
61.93	(530)/[001]	17	204	19.4
38.94	(221)/[ $\bar{1}10$ ]	9	72	13.7
50.48	(332)/[ $\bar{1}10$ ]	11	176	20.3
70.53	(111)/[ $\bar{1}10$ ]	3	48	14.8
93.37	(223)/[ $\bar{1}10$ ]	17	136	17.9
109.47	(112)/[ $\bar{1}10$ ]	3	72	16.3
121.01	(225)/[ $\bar{1}10$ ]	33	132	13.2
129.52	(113)/[ $\bar{1}10$ ]	11	88	15.2
141.06	(114)/[ $\bar{1}10$ ]	9	144	19.3

fail to reproduce the energetics and atomic arrangements of GBs with accuracy of DFT calculations [18,19], since their empirical parameters are usually adjusted to reproduce basic properties of reference bulk structures.

To reveal an origin of excess vibrational entropies at GBs, we performed first-principles lattice dynamics with the harmonic approximation. MgO was selected as a model system; it is a representative ionic crystal with the rock-salt structure, and thus results obtained from GBs in MgO would be highly transferable to various ionic systems. Fourteen symmetric tilt GBs with various structural units were systematically examined. To determine GB features governing the excess vibrational entropies, calculated vibrational entropies were then correlated to excess internal energies, excess volumes, and further local bond-length changes at the GBs.

## II. COMPUTATIONAL PROCEDURES

Energy minimizations were performed using DFT calculations of the projector augmented wave (PAW) method implemented in the VASP code [20–22]. The generalized-gradient approximation for exchange-correlation interactions was employed with the formulation parametrized by Perdew, Burke, and Ernzerhof (GGA-PBE) [23]. An energy cutoff of plane waves was set at 450 eV. Electrons of  $3s^2$  for Mg and  $2s^2 2p^4$  for O were treated as valence electrons in the PAW pseudopotentials [24,25]. A first Brillouin zone was sampled using the Monkhorst-Pack scheme [26], and a  $4 \times 4 \times 4$   $k$ -point mesh was used for a conventional cell of MgO.

A convergence criterion of self-consistent one-electron energies was set at  $10^{-6}$  eV for structural optimization and  $10^{-8}$  eV for electronic cycles in lattice dynamics calculations, respectively. A Davidson-block iteration scheme was used to improve numerical stability and thereby energy convergence. For structural optimization, atomic positions were relaxed until a force on each atom was less than  $10^{-2}$  eV/Å. With these computational conditions, the lattice constant of MgO was calculated to be 4.23 Å, in agreement with experimentally measured value of 4.21 Å [27]. Higher energy cutoffs and more  $k$ -point meshes resulted in little variations in lattice constant up to  $9 \times 10^{-3}$  Å. The band gap was calculated to

be approximately 5.3 eV, similar to a calculated value in the literature [28], although the underestimation of the band gap was observed due to the limitation of DFT calculations.

Table I summarizes the crystallographic characteristics of the GBs and details of each supercell. Symmetric tilt GBs are crystallographically defined by a common rotation axis and a misorientation angle ( $2\theta$ ) of two grains. In this work, the [001] and [ $\bar{1}10$ ] systems were examined by systematically varying  $2\theta$ . The table also lists their  $\Sigma$  values, which represent the inverse of the density of coincidence site lattice (CSL) points [29]. A GB with a low  $\Sigma$  value (e.g.,  $\Sigma = 3$  and 5) contains many CSL points in its CSL unit cell, and its GB structure typically has crystallographically simple structural units. In this work, GBs with  $\Sigma$  values from 3 to 33 were examined to cover different GB crystallographic characteristics.

Two equivalent GBs were introduced to satisfy periodic boundary conditions, and they were separated by more than 12 Å (see Table I). To find the globally energy-minimum structure of each GB, inequivalent initial atomic configurations were generated by translating one grain with respect to the other in two in-plane directions, in an increment of 0.5 Å. All the initial configurations were then statically relaxed and compared with respect to zero-temperature GB energy that does not involve a lattice vibrational contribution. This approach to finding energy-minimum atomic configurations is known as the  $\gamma$ -surface approach [30], which enables the evaluation of a potential energy surface as functions of the rigid-body translations of one grain in the case of GBs.

The energy-minimum structure of each GB was used as a reference structure for lattice dynamics calculations. The stable and metastable structures obtained are in the Supplemental Material [31].

Lattice vibrational analyses based on the finite displacement method were performed using the phonopy code [32]. Force constants were calculated from the Hellmann-Feynman forces by imposing a displacement of 0.1 Å to each atom. In this calculation, we used supercells whose lattice parameters are equal to or larger than those of a  $2 \times 2 \times 2$  supercell of the unit cell of MgO.

To calculate an excess vibrational entropy per GB area  $\Delta S_{\text{GB}}^{\text{vib}}$  and a GB free energy  $\sigma_{\text{GB}}$ , which involves lattice

vibrational contribution, thermodynamics- and statistical-mechanics-based equations were employed, as described below. Here  $\sigma_{\text{GB}}$  was assumed to be equal to an increase in Helmholtz free energy  $F$  from the perfect crystal. With the vibrational internal energy  $E^{\text{vib}}$  and vibrational entropy  $S^{\text{vib}}$ ,  $F$  is expressed as

$$F = E^{\text{static}} + F^{\text{vib}} = E^{\text{static}} + E^{\text{vib}} - TS^{\text{vib}}, \quad (1)$$

where  $E^{\text{static}}$  is the zero-temperature total energy calculated with DFT calculations. The vibrational free energy  $F^{\text{vib}}$  is given by

$$F^{\text{vib}} = \sum_i \left[ \frac{1}{2} \hbar \omega_i + k_B T \ln \left\{ 1 - \exp \left( -\frac{\hbar \omega_i}{k_B T} \right) \right\} \right], \quad (2)$$

where  $\hbar$  is the reduced Planck constant,  $\omega_i$  is the vibrational frequency of the  $i$ th normal mode, and  $k_B$  is the Boltzmann constant. The negative of the derivative of  $F^{\text{vib}}$  with respect to  $T$  is equal to the vibrational entropy  $S^{\text{vib}}$ , as

$$\begin{aligned} S^{\text{vib}} &= -\frac{\partial F^{\text{vib}}}{\partial T} \\ &= \frac{1}{2T} \sum_i \hbar \omega_i \coth \left( \frac{\hbar \omega_i}{2k_B T} \right) \\ &\quad - k_B \sum_i \ln \left[ 2 \sinh \left( \frac{\hbar \omega_i}{2k_B T} \right) \right]. \end{aligned} \quad (3)$$

Furthermore,  $S^{\text{vib}}$  was divided into  $S_{\mu,j}^{\text{vib}}$ , the atom-projected vibrational entropy of the  $\mu$ th atom for the  $j$ th degree of freedom, as follows:

$$\begin{aligned} S_{\mu,j}^{\text{vib}} &= \frac{1}{2T} \sum_i |e_i(\mathbf{k}, \mu; j)|^2 \hbar \omega_i \coth \left( \frac{\hbar \omega_i}{2k_B T} \right) \\ &\quad - k_B \sum_i |e_i(\mathbf{k}, \mu; j)|^2 \ln \left[ 2 \sinh \left( \frac{\hbar \omega_i}{2k_B T} \right) \right], \end{aligned} \quad (4)$$

where  $e_i(\mathbf{k}, \mu; j)$  is the  $i$ th Cartesian component of a polarization vector. To quantify the atom-projected vibrational entropy of the  $\mu$ th atom  $S_{\mu}^{\text{vib}}$ , the sum over  $3N$  degrees of freedom  $S_{\mu}^{\text{vib}} = \sum_{j=1}^{3N} S_{\mu,j}^{\text{vib}}$  was then computed. The sum of  $S_{\mu}^{\text{vib}}$  over all atoms is equal to  $S^{\text{vib}}$ . Finally  $\sigma_{\text{GB}}$  was calculated by

$$\sigma_{\text{GB}} = (F_{\text{GB}} - F_{\text{BULK}})/2A, \quad (5)$$

where  $F_{\text{GB}}$  and  $F_{\text{BULK}}$  are the Helmholtz free energies of a GB structure and the perfect-crystal structure of MgO, respectively, and  $A$  is the GB area. The term  $\sigma_{\text{GB}}$  was divided into three terms:

$$\sigma_{\text{GB}} = \Delta E_{\text{GB}}^{\text{static}} + \Delta E_{\text{GB}}^{\text{vib}} - T \Delta S_{\text{GB}}^{\text{vib}}, \quad (6)$$

where  $\Delta E_{\text{GB}}^{\text{static}}$  is the excess internal energy per GB area at 0 K without vibrational contribution. This term was calculated from the total-energy difference between a GB structure and the perfect crystal.  $\Delta E_{\text{GB}}^{\text{vib}}$  is the excess vibrational internal energy per GB area. Each term on the right side was calculated as a difference between the corresponding values of a GB and the perfect crystal.

In our test calculations, both the harmonic and quasiharmonic approximation were applied to the most stable structure of the  $\Sigma 5(310)/[001]$  to investigate the contribution of

thermal expansion to  $\sigma_{\text{GB}}$ . Differences between  $\sigma_{\text{GB}}$  obtained from the two approximations were found to be less than  $9 \times 10^{-3} \text{ J/m}^2$  up to around 1000 K, although at above 1200 K physically reasonable free energies were not obtained from the quasiharmonic approximation due to the large elongation of the GB structure at negative pressures above  $-12 \text{ GPa}$ . For this reason, only the harmonic approximation was applied to the 14 GBs studied. These results are contained in Sec. S1 in the Supplemental Material [31].

### III. RESULTS AND DISCUSSION

#### A. Most stable and metastable GB structures

Figure 1 displays the most stable GB structures obtained from DFT calculations. As examples, the structural units of  $\Sigma 5(310)/[001]$  and  $\Sigma 3(111)/[\bar{1}10]$  are indicated by the shapes with a black edge. A structural unit is a repeated pattern of atomic arrangements at a GB in the in-plane direction, although its definition is somewhat arbitrary. The obtained structural units are found to vary depending on the misorientation angles and rotational axes, having several similar features of atomic arrangements: for the  $[001]$  system [Fig. 1(a)], the GBs tend to have ‘‘open’’ atomic structures, involving an empty space at the boundary planes and lower coordination than sixfold coordination. Among these GBs, the atomic structures of  $\Sigma 5(210)/[001]$ ,  $\Sigma 5(310)/[001]$ , and  $\Sigma 25(710)/[001]$  were reported by previous atomistic simulations and DFT calculations [28,33–35], which are in good agreement with the present results.

Figure 1(b) shows stable GB structures for the  $[\bar{1}10]$  system. For the  $\Sigma 9(221)/[\bar{1}10]$ ,  $\Sigma 11(332)/[\bar{1}10]$ ,  $\Sigma 17(223)/[\bar{1}10]$ , and  $\Sigma 11(113)/[\bar{1}10]$ , the projected image makes Mg and O ions at the GB planes look unphysically close to each other, but their actual distance is 2.0–2.1 Å; one grain is translated relative to the other grain with  $a/2$  along the  $[\bar{1}10]$  axis, where  $a$  is the lattice constant of the conventional cell of MgO. For the  $\Sigma 3(112)/[\bar{1}10]$ ,  $\Sigma 33(225)/[\bar{1}10]$ , and  $\Sigma 9(114)/[\bar{1}10]$ , no rigid body translation along the  $[\bar{1}10]$  axis occurs between two grains, with 1.8–1.9 Å of spacing between two grains perpendicular to the boundary planes. These types of structural units with the  $[\bar{1}10]$  rotational axis, with open structures and translation along the axis, were also reported by previous atomistic simulations [35,36]. The  $\Sigma 3(111)/[\bar{1}10]$  corresponds to a coherent twin GB, with a bulklike atomic arrangement.

Metastable structures were also determined to examine their relative stability to the most stable structures at a finite temperature, as Najafabadi *et al.* indicated that the most stable GB structures changed with temperature for twist GBs in Au [14]. Figure 2 shows metastable structures of four GBs obtained. For the metastable structures of the  $\Sigma 5(310)/[001]$ ,  $\Sigma 17(530)/[001]$ ,  $\Sigma 3(112)/[\bar{1}10]$ , and  $\Sigma 11(113)/[\bar{1}10]$ ,  $\Delta E_{\text{GB}}^{\text{static}}$  are calculated to be 0.23, 0.07, 0.07, and 0.04 J/m<sup>2</sup> higher than those of their most stable structures, respectively. For the  $\Sigma 5(310)/[001]$  and  $\Sigma 17(530)/[001]$ , the metastable structures do not have open spaces as is formed for the most stable structures [Fig. 1(a)], but they have ‘‘dense’’ structures at which ions are closely packed. Similar dense structures were also predicted

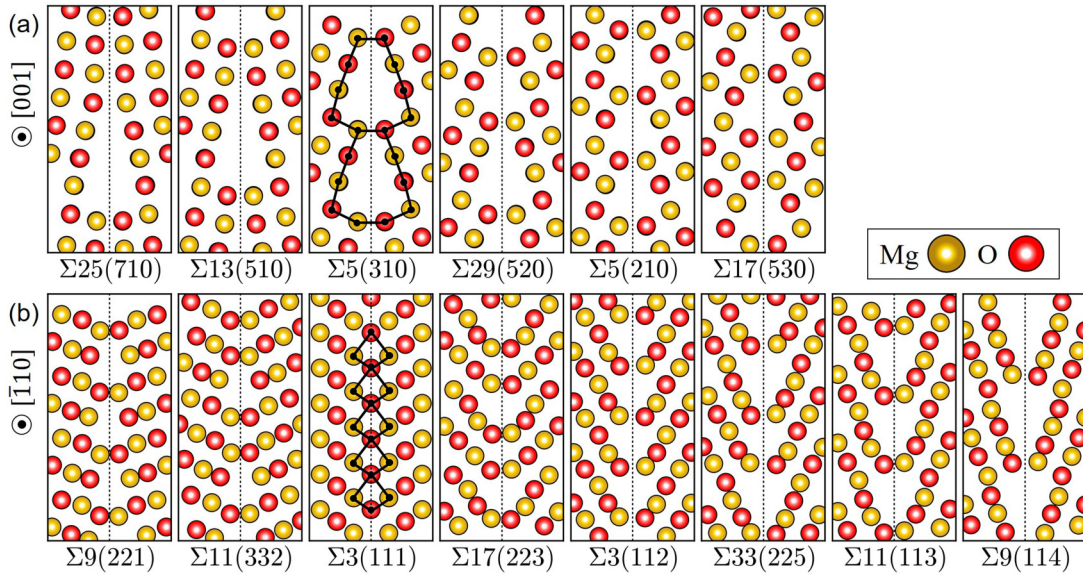


FIG. 1. Most stable structures of all the calculated GBs with (a) the [001] and (b)  $[\bar{1}10]$  rotational axes. The dashed line corresponds to the boundary plane. The yellow and red balls represent Mg and O ions, respectively. For the  $\Sigma 5(310)/[001]$  and  $\Sigma 3(111)/[\bar{1}10]$ , examples of structural units are indicated by the black line and dots.

as metastable structures in the literature [36,37]. For the metastable structures of the  $\Sigma 3(112)/[\bar{1}10]$  and  $\Sigma 11(113)/[\bar{1}10]$ , one grain is displaced by  $a/2$  along the  $[\bar{1}10]$  axis with respect to the other grain. Although the other GBs also had metastable structures, their atomic arrangements showed similar features to the four metastable structures mentioned above. The four GB structures in Fig. 2 were thus used as representatives of metastable structures for lattice dynamics calculations.

### B. Excess free energy and excess vibrational entropy

Figure 3 shows  $\sigma_{\text{GB}}$  and its vibrational components (i.e.,  $\Delta E_{\text{GB}}^{\text{vib}}$  and  $T\Delta S_{\text{GB}}^{\text{vib}}$ ) for the  $\Sigma 5(310)/[001]$ . At up to around 100 K,  $\Delta E_{\text{GB}}^{\text{vib}}$  and  $T\Delta S_{\text{GB}}^{\text{vib}}$  are much smaller than  $\Delta E_{\text{GB}}^{\text{static}}$ , indicating that temperature dependence of  $\sigma_{\text{GB}}$  is insignificant. At  $T \geq 100$  K,  $\sigma_{\text{GB}}$  decreases with rising temperature as  $T\Delta S_{\text{GB}}^{\text{vib}}$  becomes comparable to  $\sigma_{\text{GB}}$  at 0 K, whereas  $\Delta E_{\text{GB}}^{\text{vib}}$  is still smaller than  $\Delta E_{\text{GB}}^{\text{static}}$  and also nearly constant. The temperature dependence of  $\sigma_{\text{GB}}$  thus originates from  $T\Delta S_{\text{GB}}^{\text{vib}}$ . Since the same trend was observed for the other GBs, the

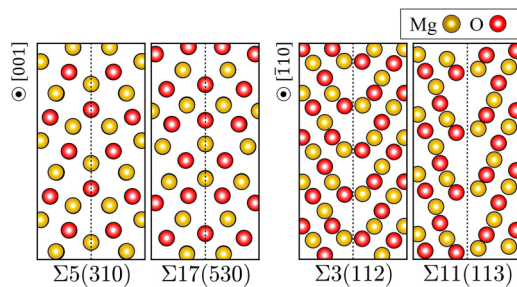


FIG. 2. Metastable GB structures for the  $\Sigma 5(310)/[001]$ ,  $\Sigma 17(530)/[001]$ ,  $\Sigma 3(112)/[\bar{1}10]$ , and  $\Sigma 11(113)/[\bar{1}10]$ . The dashed line represents the boundary plane.

discussion below focuses on only  $\Delta S_{\text{GB}}^{\text{vib}}$  for contribution of lattice vibration to  $\sigma_{\text{GB}}$ .

Figure 4 displays  $\sigma_{\text{GB}}$  as a function of temperature. Although  $\sigma_{\text{GB}}$  tends to decrease with rising temperature for all GBs, the temperature dependence of  $\sigma_{\text{GB}}$  varies depending on each GB. For instance, the  $\Sigma 25(710)/[001]$  has a larger  $\sigma_{\text{GB}}$  of  $1.33 \text{ J/m}^2$  than the  $\Sigma 5(210)/[001]$  ( $\sigma_{\text{GB}} = 1.26 \text{ J/m}^2$ ) at 0 K, whereas at 1500 K, the  $\Sigma 25(710)/[001]$  is thermodynamically more stable ( $\sigma_{\text{GB}} = 1.13 \text{ J/m}^2$ ) than the  $\Sigma 5(210)/[001]$  ( $\sigma_{\text{GB}} = 1.15 \text{ J/m}^2$ ). As plotted with the blue line in Fig. 4, the metastable structures of  $\Sigma 17(530)/[001]$

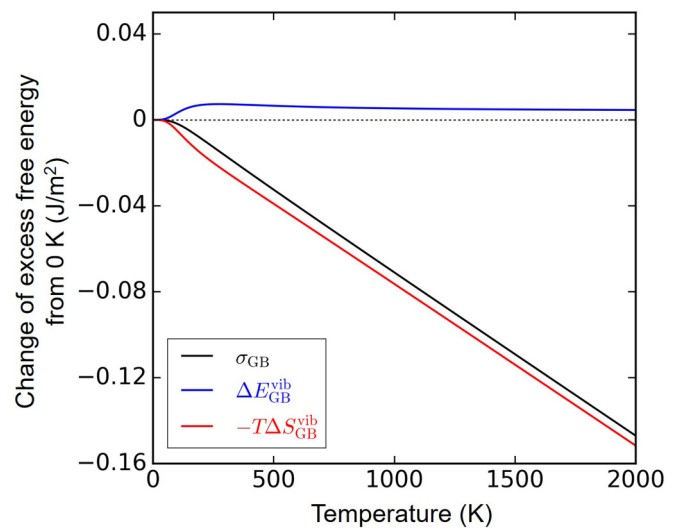


FIG. 3. Change of the GB free energy ( $\sigma_{\text{GB}}$ ) from 0 K for the  $\Sigma 5(310)/[001]$ . The black, red and blue lines represent  $\sigma_{\text{GB}}$ , the excess vibrational internal energy per GB area ( $\Delta E_{\text{GB}}^{\text{vib}}$ ) and the excess vibrational entropy per GB area multiplied by temperature ( $-T\Delta S_{\text{GB}}^{\text{vib}}$ ), respectively.

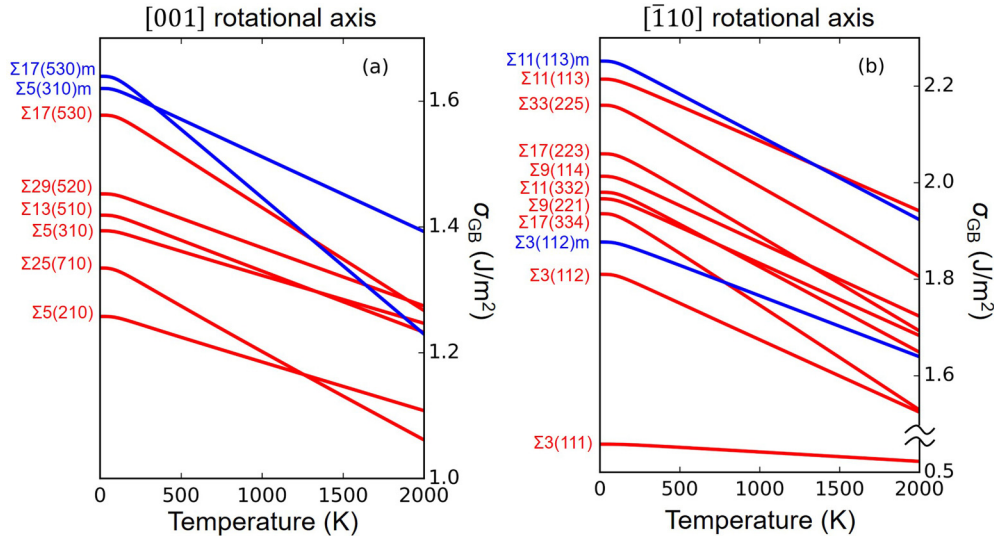


FIG. 4. GB free energy ( $\sigma_{GB}$ ) as a function of temperature  $T$  for the GBs with (a) the [001] and (b)  $[\bar{1}10]$  rotational axes. The red and blue lines represent  $\sigma_{GB}$  for the most stable and metastable GBs, respectively.

and  $\Sigma 17(334)/[\bar{1}10]$  (denoted as “ $\Sigma 17(530)/[001]m$ ” in Fig. 4, for instance) also have large  $\Delta S_{GB}^{vib}$ , resulting in a rapid decrease in  $\sigma_{GB}$  from 1.58 to 1.27  $\text{J}/\text{m}^2$  and from 1.94 to 1.53  $\text{J}/\text{m}^2$  between  $T = 0$ –2000 K, respectively. A comparison between  $\Delta S_{GB}^{vib}$  of the [001] and  $[\bar{1}10]$  systems indicates that the magnitude of  $\Delta S_{GB}^{vib}$  does not depend on the rotational axis, while  $\Delta E_{GB}^{static}$  is entirely larger for the  $[\bar{1}10]$  GBs. Therefore, GBs in MgO polycrystals are most likely to have a wide spectrum of  $\Delta S_{GB}^{vib}$ , depending on their individual GB structures. Such a temperature dependence may also affect the population of individual GBs in polycrystalline microstructures at a given temperature, as it was reported that GBs with particular interfacial planes were observed more frequently than other GBs in polycrystalline MgO [38,39].

The relative stability of stable and metastable structures for the crystallographically same GB is also found to change depending on temperature. For the  $\Sigma 17(530)/[001]$  and  $\Sigma 11(113)/[\bar{1}10]$ , the most stable structures change at 1300 and 1350 K, respectively, as the metastable structures at 0 K has larger  $\Delta S_{GB}^{vib}$  than the most stable structures at 0 K. By contrast, the metastable structures of the  $\Sigma 5(310)/[001]$  and  $\Sigma 3(112)/[\bar{1}10]$  at 0 K have smaller  $\Delta S_{GB}^{vib}$  than those of the most stable structures, and thus have their higher values of  $\sigma_{GB}$  even at 2000 K. In the present study, we examine only four metastable structures of symmetric tilt GBs with low- $\Sigma$  values. The numbers of metastable structures for a GB would increase with its  $\Sigma$  value, since the periodicity of the structural unit along the boundary plane becomes longer with increasing  $\Sigma$  value, involving various types of atomic arrangement. GBs with a high- $\Sigma$  value may thus often experience stable-metastable transition depending on temperatures.

For the  $\Sigma 17(530)/[001]$  and  $\Sigma 11(113)/[\bar{1}10]$ , transformation between the stable and metastable structures (see Figs. 1 and 2) involves not only a change in atomic arrangement but also rigid body translation along the rotational axis. Such translation is likely to have a large activation energy, since relative shifts of one grain are required. Thus, when a GB structure is formed at a high temperature and then annealed,

the high-temperature GB structure may be retained even at low temperature.

In this work we used only static calculations, and thus the GB transition cannot occur simultaneously in our simulations. The GB transition may occur in long-timescale molecular dynamics (MD) simulations. Although such DFT-MD simulations still have high computational cost, they would be employed in the combination of lattice dynamics calculations in future works.

A previous atomistic simulation study of MgO showed that a difference of  $\sigma_{GB}$  at 300 and 1200 K was as small as 0.05  $\text{J}/\text{m}^2$  for the  $\Sigma 5(210)/[001]$  [16]. In this study the  $\Sigma 5(210)/[001]$  shows a difference of 0.04  $\text{J}/\text{m}^2$  between the two temperatures, comparable to the previous result. On the other hand, the  $\Sigma 25(710)/[001]$  shows a difference of 0.13  $\text{J}/\text{m}^2$ , three times larger than that of the  $\Sigma 5(210)/[001]$ . Although the difference of 0.13  $\text{J}/\text{m}^2$  is still smaller than the pressure contribution to  $\sigma_{GB}$  at high pressures reaching tens of GPa, as indicated in the previous study [16], this value is not negligible in normal conditions. Comparing with a previous study of the  $\Sigma 5(310)/[001]$  in Al [13], the  $\Sigma 5(310)/[001]$  in MgO studied exhibits approximately by five times a smaller value of  $\Delta S_{GB}^{vib}$  ( $8 \times 10^{-5} \text{ J}/\text{m}^2 \text{ K}^{-1}$ ) than that in Al ( $4 \times 10^{-4} \text{ J}/\text{m}^2 \text{ K}^{-1}$ ). Although the previous study used a Morse-type interatomic potential and thus a direct comparison to our result is difficult,  $\Delta S_{GB}^{vib}$  may affect  $\sigma_{GB}$  more significantly for Al than MgO. Our future work with DFT calculations will address  $\Delta S_{GB}^{vib}$  of metal GBs by varying their misorientation angles to reveal the difference in  $\Delta S_{GB}^{vib}$  between Al, MgO and covalent crystals such as Si.

### C. Correlation of excess vibrational entropy to excess internal energy and excess volume

To reveal a physical origin of the excess vibrational entropies generated by the GBs, correlations of  $\Delta S_{GB}^{vib}$  to  $\Delta E_{GB}^{static}$  and excess volume  $\Delta V_{GB}$  were investigated;  $\Delta V_{GB}$  represents a volume increase at a GB with respect to the volume in bulk,

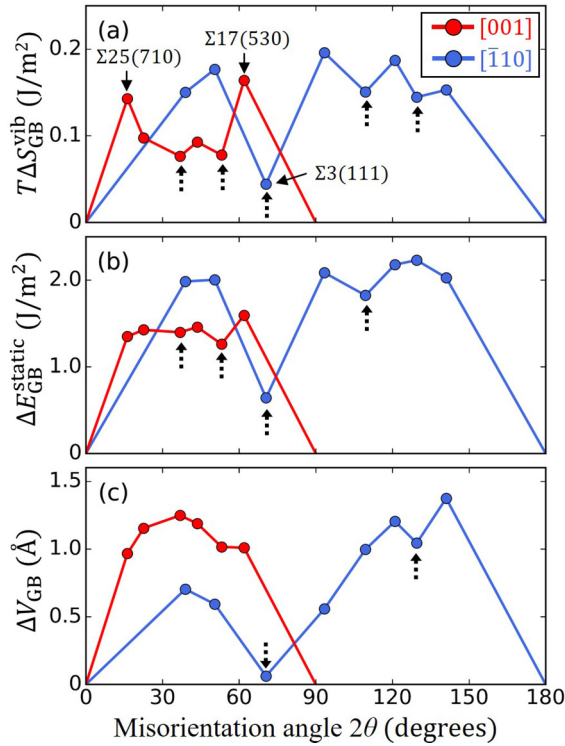


FIG. 5. (a) Excess vibrational entropy  $T\Delta S_{\text{GB}}^{\text{vib}}$  ( $T = 1000$  K), (b) excess static energy  $\Delta E_{\text{GB}}^{\text{static}}$ , and (c) excess volume  $\Delta V_{\text{GB}}$  as a function of misorientation angle  $2\theta$ . The black dashed arrow indicates the cusp position.

and is often used to discuss the correlation to  $\sigma_{\text{GB}}$  at 0 K [9,11]. For instance, Najafabadi *et al.* showed a rough correlation between  $\Delta V_{\text{GB}}$  and  $\sigma_{\text{GB}}$  in Au GBs [14]. Figures 5(a) and 5(b) show  $T\Delta S_{\text{GB}}^{\text{vib}}$  ( $T = 1000$  K) and  $\Delta E_{\text{GB}}^{\text{static}}$  as a function of the misorientation angle, respectively. The two quantities seem to change with  $2\theta$  in the same manner, although there exist differences in cusp positions and relative values. For the [001] system,  $T\Delta S_{\text{GB}}^{\text{vib}}$  has clear local maxima at  $16.26^\circ$  for the  $\Sigma 25(710)/[001]$  and  $61.93^\circ$  for the  $\Sigma 17(530)/[001]$ , whereas  $\Delta E_{\text{GB}}^{\text{static}}$  has one local maxima at  $61.93^\circ$ . For the  $[\bar{1}10]$  system,  $T\Delta S_{\text{GB}}^{\text{vib}}$  has three cusps at  $70.53^\circ$ ,  $109.47^\circ$ , and  $129.52^\circ$  for the  $\Sigma 3(111)/[\bar{1}10]$ ,  $\Sigma 3(112)/[\bar{1}10]$ , and  $\Sigma 11(113)/[\bar{1}10]$ , respectively, whereas  $\Delta E_{\text{GB}}^{\text{static}}$  has two cusps at  $70.53^\circ$  and  $109.47^\circ$ . As shown in Fig. 6(a), the correlation between

$T\Delta S_{\text{GB}}^{\text{vib}}$  and  $\Delta E_{\text{GB}}^{\text{static}}$  is relatively strong with a correlation coefficient of 0.85. Even without the  $\Sigma 3(111)/[\bar{1}10]$ , which corresponds to a coherent twin GBs and is energetically much stable ( $\Delta E_{\text{GB}}^{\text{static}} = 0.64$  J/m<sup>2</sup>), the correlation coefficient for the other GBs is calculated to be 0.78. However, without the  $\Sigma 3(111)/[\bar{1}10]$ , the correlation coefficients for the [001] and  $[\bar{1}10]$  rotational axes are 0.60 and 0.26, respectively. Therefore although  $\Delta E_{\text{GB}}^{\text{static}}$  as a whole is correlated with  $\Delta S_{\text{GB}}^{\text{vib}}$ , the strength of the correlation differ with the rotational axes.

A comparison between  $\Delta V_{\text{GB}}$  [Fig. 5(c)] and  $\Delta S_{\text{GB}}^{\text{vib}}$  [Fig. 5(a)] indicates clear differences in both cusp positions and relative values. For the [001] rotational axis,  $\Delta V_{\text{GB}}$  increases up to  $36.87^\circ$  for the  $\Sigma 5(310)/[001]$  and then monotonically decreases, without any cusps. For the  $[\bar{1}10]$  rotational axis,  $\Delta V_{\text{GB}}$  has two cusps at  $70.53^\circ$  and  $129.52^\circ$ . In addition, the values of  $\Delta V_{\text{GB}}$  at  $2\theta \leq 70.53^\circ$  are entirely smaller than at  $2\theta > 70.53^\circ$ . This tendency is not observed for  $\Delta S_{\text{GB}}^{\text{vib}}$ . Figure 6(b) shows that  $\Delta V_{\text{GB}}$  and  $\Delta S_{\text{GB}}^{\text{vib}}$  are less correlated with a correlation coefficient of 0.11 and  $-0.49$  with and without the  $\Sigma 3(111)/[\bar{1}10]$ , suggesting that a local volume increase at a GB is not a critical factor in determining the magnitude of  $\Delta S_{\text{GB}}^{\text{vib}}$ .

We note that  $\sigma_{\text{GB}}$  and  $V_{\text{GB}}$  are also not well correlated, as shown in Fig. 6(c). The reason is that in MgO, stable GB structures have both small and large  $V_{\text{GB}}$ , strongly depending on the crystallographic characteristics of GBs. The formation of structural units with various  $V_{\text{GB}}$  is clearly due to the fact that even at GBs, the Coulomb interaction, as well as the bulk crystal structure (here the rock-salt structure), is a critical factor in determining stable ionic arrangements, as  $\text{Mg}^{2+}$  and  $\text{O}^{2-}$  are bonded across the GB plane for the “open” structures (see Fig. 1). This trend clearly differs from fcc metals: their stable structural units are basically “dense” and do not have open structures as is found at the  $\Sigma 5(310)/[001]$  in MgO [10,40,41]. For GBs in fcc metals,  $V_{\text{GB}}$  is thus relatively correlated with strain energies at GBs and thereby their GB energies, as was indicated in the literature [9].

#### D. Correlation of excess vibrational entropy to bond-length change

Since  $\Delta S_{\text{GB}}^{\text{vib}}$  is fundamentally caused by thermal vibration of atoms, involving variation in interatomic bond length,

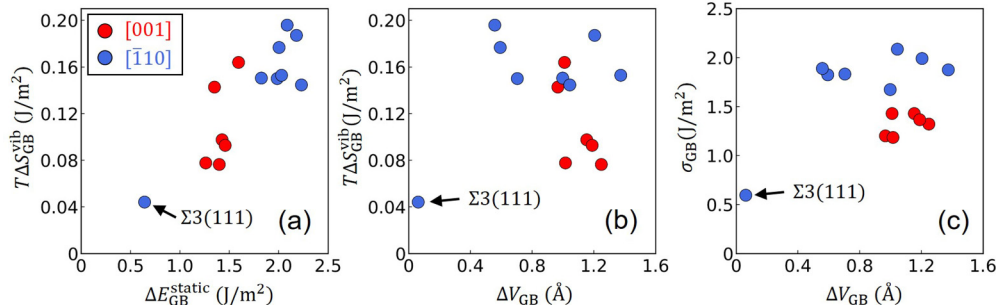


FIG. 6. Correlation between  $T\Delta S_{\text{GB}}^{\text{vib}}$  ( $T = 1000$  K) and (a)  $\Delta E_{\text{GB}}^{\text{static}}$  and (b)  $\Delta V_{\text{GB}}$ , and (c) the correlation between  $\sigma_{\text{GB}}$  and  $\Delta V_{\text{GB}}$ . The red and blue points represent the GBs with the [001] and  $[\bar{1}10]$  rotational axes, respectively.

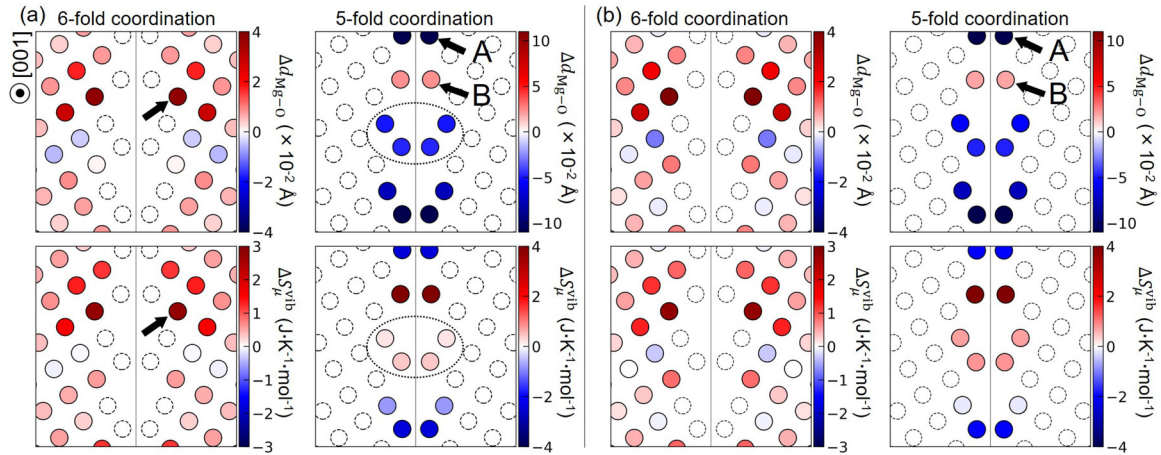


FIG. 7. Bond-length change  $\Delta d_{\text{Mg-O}}$  and vibrational entropy change  $\Delta S_{\mu}^{\text{vib}}$  ( $T = 1000$  K) from the perfect crystal for each (a) Mg ion and (b) O ion for the  $\Sigma 17(530)/[001]$ . The results of ions sixfold and fivefold coordinations are displayed. The Mg or O column positions at the GB are displayed with the dashed line circles. The fivefold coordinated ions with large negative and positive  $T\Delta S_{\mu}^{\text{vib}}$  are labeled A and B, respectively. For these labeled ions, the partial phonon density of states is plotted in Fig. 8.

correlations between bond lengths between nearest neighboring Mg and O ions and  $\Delta S_{\text{GB}}^{\text{vib}}$  were examined. Figure 7 shows bond-length changes  $\Delta d_{\text{Mg-O}}$  and  $T\Delta S_{\mu}^{\text{vib}}$  of each ion with sixfold and fivefold coordination at the  $\Sigma 17(530)/[001]$  for Mg [Fig. 7(a)] and O [Fig. 7(b)]. Here  $\Delta d_{\text{Mg-O}}$  were obtained from differences of Mg-O bond lengths near a GB from that in the perfect crystal. It is seen that the sixfold coordinated Mg ions with positive  $\Delta d_{\text{Mg-O}}$  have positive  $\Delta S_{\mu}^{\text{vib}}$ , whereas those with negative  $\Delta d_{\text{Mg-O}}$  have negative  $\Delta S_{\mu}^{\text{vib}}$ . A similar trend is also found for the fivefold coordinated Mg ions, although the Mg ions encircled with the dotted line seemingly have negative  $\Delta d_{\text{Mg-O}}$  while exhibit positive  $\Delta S_{\mu}^{\text{vib}}$ . This will be addressed later in Fig. 9. For the O ions [Fig. 7(b)], the correlation between  $\Delta d_{\text{Mg-O}}$  and  $\Delta S_{\mu}^{\text{vib}}$  is very similar to that for the Mg ions, as the atomic arrangements of O ions are almost the same as Mg ions, having translation symmetry even at the GBs.

To reveal how bond-length changes at GBs affect  $\Delta S_{\mu}^{\text{vib}}$ , partial phonon densities of states (DOS) for the ions labeled A and B in Fig. 7 is plotted in Fig. 8. For the Mg(A) ion [Fig. 8(a)], with a shorter Mg-O bond length, the DOS shifts toward high-frequency modes from that in the perfect crystal, clearly decreasing the peaks at 7.9 and 12.1 THz. The peak at a high frequency of 21.5 THz also appears. The shift toward high-frequency modes causes  $S_{\mu}^{\text{vib}}$  to decrease, since  $S_{\mu}^{\text{vib}}$  decreases with increasing characteristic frequency, as described by Eq. (3). Such a shift physically means that an ion with a shorter bond length at a GB has a larger spring constant than an ion in the perfect crystal, and thus its displacement from the equilibrium position becomes small, leading to a decrease in accessible atomic position for the ion. For the Mg(B) ion, with a longer bond length, its DOS entirely shifts toward low-frequency modes with decreases in the high-frequency modes at 12.1 and 17.5 THz. The peak at 7.9 THz observed in the perfect crystal still remains, with a slightly shift to 7.5 THz. These results indicate that the lattice vibration of the Mg(B) ion becomes “loose,” leading to large atomic displacements and thereby increased accessible atomic positions.

As seen in Fig. 8(b), the labeled O ions also show similar shifts to the labeled Mg ions, although their peak positions and intensities differ. The O(A) ion has a strong peak at 21.4 THz, with the decreases of the DOS at 12.1 and 17.4 THz that are observed in the perfect crystal (dashed black line). For the O(B) ion the two peaks become weak, shifting toward low frequencies. These differences between the DOS of the Mg and O ions probably result from the difference between their atomic masses, since O ions vibrate with higher frequencies and thus their DOS is distributed entirely at higher frequencies than that of the Mg ions. Considering that  $S_{\mu}^{\text{vib}}$  monotonically increases with decreasing phonon frequency [see Eq. (4)], GB ions with longer bond lengths are a critical factor in decreasing phonon frequencies and thereby increasing  $S_{\mu}^{\text{vib}}$ .

For the Mg and O ions in all the GB structures studied, the correlation between the Mg-O bond length and  $\Delta S_{\mu}^{\text{vib}}$  was examined, as shown in Fig. 9. Classifying the ions in terms of their coordination number, the two quantities are well correlated: for both Mg and O ions,  $\Delta S_{\mu}^{\text{vib}}$  linearly increases with increasing Mg-O bond length. This trend is observed for

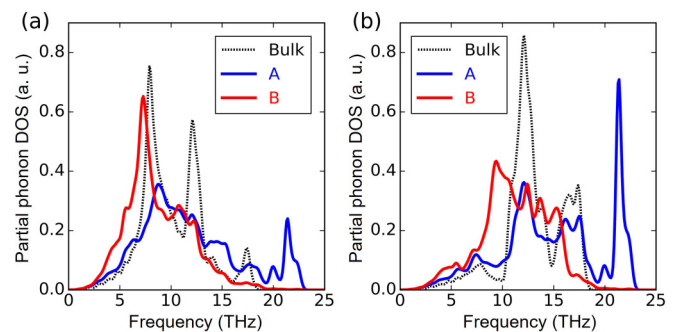


FIG. 8. Partial phonon density of states (DOS) for the labelled ions in Fig. 7 for (a) Mg and (b) O ions. The reference partial DOS for the Mg and O ion in the perfect crystal are also plotted by the black dashed lines.

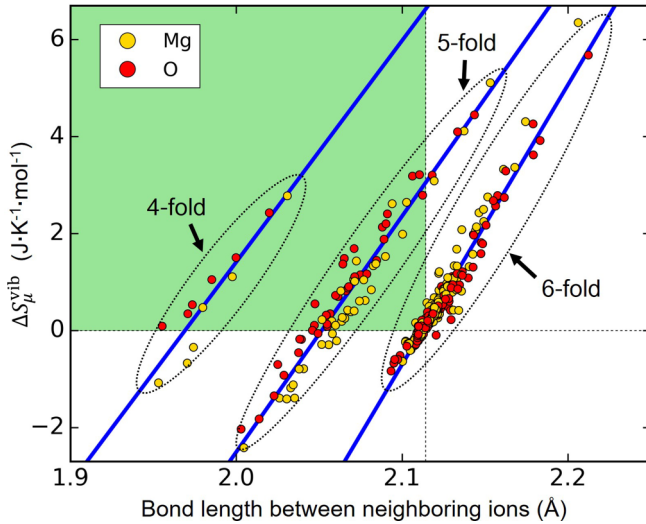


FIG. 9. Correlation between  $\Delta S_{\mu}^{\text{vib}}$  ( $T = 1000$  K) and bond length between neighboring ions for all ions in all the GB structures studied. The yellow and red data points correspond to Mg and O ions, respectively. The blue lines were obtained by fitting the data points of each coordination to linear functions. The fourfold and fivefold coordinated ions in the green area have shorter bond lengths than the sixfold coordinated ions in the perfect crystal but have positive  $\Delta S_{\mu}^{\text{vib}}$ .

all the GBs studied regardless of differences between their crystallographic characteristics and atomic arrangements. It is noted that the fourfold and fivefold coordinated ions in the green area have negative  $\Delta d_{\text{Mg-O}}$  (since their bond lengths are shorter than the sixfold coordinated ion in the perfect crystal) but these ions exhibit positive  $\Delta S_{\mu}^{\text{vib}}$ . This situation is similar to the ions encircled in Fig. 7(a). These ions, however, still clearly show a positive correlation between their bond lengths and  $\Delta S_{\mu}^{\text{vib}}$ , although the bond length at  $\Delta S_{\mu}^{\text{vib}} = 0$  differs between the coordination numbers. Considering this difference, it is likely that when a GB contains many ions with longer bond lengths than those at  $\Delta S_{\mu}^{\text{vib}} = 0$  for each coordination number, with positive  $\Delta S_{\mu}^{\text{vib}}$ , the GB exhibits a large positive  $\Delta S_{\text{GB}}^{\text{vib}}$  and hence a sharp decrease in  $\sigma_{\text{GB}}$  with temperature. By contrast, a GB containing many ions with shorter bond lengths should have a small positive  $\Delta S_{\text{GB}}^{\text{vib}}$  and thereby little temperature dependence of  $\sigma_{\text{GB}}$ .

To evaluate which coordination more dominantly affects  $\Delta S_{\text{GB}}^{\text{vib}}$ ,  $\Delta S_{\mu}^{\text{vib}}$  were fitted to linear functions (blue lines). Their slopes are calculated to be 57.7, 48.6, and 45.7  $\text{JK}^{-1} \text{mol}^{-1} \text{\AA}^{-1}$  for sixfold, fivefold, and fourfold coordination, respectively, indicating that bond-length changes of sixfold coordinated ions have larger contribution to  $\Delta S_{\text{GB}}^{\text{vib}}$ . Such ions are distributed at atomic columns surrounding a structural unit, as observed for the sixfold coordination in Fig. 7. Thus GBs involving many sixfold coordinated ions with longer bond lengths may lead to a large increase in  $\Delta S_{\text{GB}}^{\text{vib}}$ .

A systematic investigation of 14 GBs in MgO has demonstrated that bond-length changes at the GBs are well correlated with  $\Delta S_{\mu}^{\text{vib}}$  despite of the difference in GB crystallographic characteristics. Although bond lengths are here used as descriptors for excess vibrational entropies at GBs, such a correlation should originally arise from reduced force constants between atoms around GB cores. In general, reduced force constants between atoms result in their longer bond lengths. In fact, as can be seen in Fig. 8, the atoms with longer bond lengths at GB cores have smaller vibrational frequencies, indicating their softened force constants. Such reduced force constants between atoms can be realized at around GB cores, where atomic environments and their resultant chemical environments are different from those in bulk.

Although previous studies of metal GBs related  $\Delta V_{\text{GB}}$  to  $\Delta S_{\text{GB}}^{\text{vib}}$  [13,14],  $\Delta V_{\text{GB}}$  was less correlated with  $\Delta S_{\text{GB}}^{\text{vib}}$  for MgO. This difference implies that critical factors determining  $\Delta S_{\text{GB}}^{\text{vib}}$  differ depending on substances with various chemical bonding states, which may be further varied at GBs. Our future work will apply lattice dynamics calculations to GBs in other oxides, metals, and semiconductors, with the goal of uncovering the underlying physics of the excess entropy of GBs.

#### IV. CONCLUSIONS

To reveal the atomic-level origin of excess vibration entropies generated by GBs in MgO, first-principles lattice dynamics with the harmonic approximation was applied to symmetric tilt GBs for the [001] and  $[\bar{1}10]$  systems. It was found that  $\Delta S_{\text{GB}}^{\text{vib}}$  significantly varied depending on the individual GBs. For the GBs with larger  $\Delta S_{\text{GB}}^{\text{vib}}$ ,  $\sigma_{\text{GB}}$  decreased with increasing temperature more significantly than GBs with a smaller  $\Delta S_{\text{GB}}^{\text{vib}}$ . Due to the large decrease in  $\sigma_{\text{GB}}$ , the relative thermodynamic stability of the GBs changed with temperature. The zero-temperature metastable structures of the  $\Sigma 17(530)/[001]$  and  $\Sigma 11(113)/[\bar{1}10]$  were found to have larger  $\Delta S_{\text{GB}}^{\text{vib}}$  than their most stable structures at 0 K. As a result, the metastable structures became more stable at elevated temperatures, indicating that stable GB structures undergo structural transition depending on temperatures. The values of  $\Delta S_{\text{GB}}^{\text{vib}}$  were less correlated with  $\Delta V_{\text{GB}}$ , indicating that a volume increase at a GB is not necessarily a critical factor for  $\Delta S_{\text{GB}}^{\text{vib}}$ . It was found that the contribution of each ion to  $\Delta S_{\text{GB}}^{\text{vib}}$ ,  $\Delta S_{\mu}^{\text{vib}}$ , was well correlated with Mg-O bond lengths at GBs. Local bond-length changes induced by GBs, which originates from changes in bond strength, are therefore one of the critical descriptors for evaluating excess vibrational entropies generated by GBs.

#### ACKNOWLEDGMENT

This study was supported by JSPS KAKENHI Grant No. JP19H05786.

[1] Y. Qi and P. E. Krajewski, Molecular dynamics simulations of grain boundary sliding: The effect of stress and boundary misorientation, *Acta Mater.* **55**, 1555 (2007).

[2] H. Somekawa and T. Mukai, Effect of grain boundary structures on grain boundary sliding in magnesium, *Mater. Lett.* **76**, 32 (2012).

- [3] D. W. Readey and R. E. Jech, Energies and grooving kinetics of [001] tilt boundaries in nickel oxide, *J. Am. Ceram. Soc.* **51**, 201 (1968).
- [4] H. Miura, M. Kato, and T. Mori, Temperature dependence of the energy of Cu [110] symmetric tilt grain boundaries, *J. Mater. Sci. Lett.* **13**, 46 (1994).
- [5] A. Tsoga and P. Nikolopoulos, Surface and grain-boundary energies in yttria-stabilized zirconia (YSZ-8 mol%), *J. Mater. Sci.* **31**, 5409 (1996).
- [6] S. J. Dillon, M. P. Harmer, and G. S. Rohrer, The relative energies of normally and abnormally growing grain boundaries in alumina displaying different complexions, *J. Am. Ceram. Soc.* **93**, 1796 (2010).
- [7] M. N. Kelly, S. A. Bojarski, and G. S. Rohrer, The temperature dependence of the relative grain-boundary energy of yttria-doped alumina, *J. Am. Ceram. Soc.* **100**, 783 (2017).
- [8] M. N. Kelly, W. Rheinheimer, M. J. Hoffmann, and G. S. Rohrer, Anti-thermal grain growth in SrTiO<sub>3</sub>: Coupled reduction of the grain boundary energy and grain growth rate constant, *Acta Mater.* **149**, 11 (2018).
- [9] D. Wolf, Structure-energy correlation for grain boundaries in F.C.C. metals—III. Symmetrical tilt boundaries, *Acta Metall. Mater.* **38**, 781 (1990).
- [10] J. D. Rittner and D. N. Seidman, (110) symmetric tilt grain-boundary structures in fcc metals with low stacking-fault energies, *Phys. Rev. B* **54**, 6999 (1996).
- [11] D. L. Olmsted, S. M. Files, and E. A. Holm, Survey of computed grain boundary properties in face-centered cubic metals: I. Grain boundary energy, *Acta Mater.* **57**, 3694 (2009).
- [12] S. Patanaphan, D. L. Olmsted, V. V. Bulatov, E. A. Holm, A. D. Rollett, and G. S. Rohrer, Grain boundary energies in body-centered cubic metals, *Acta Mater.* **88**, 346 (2015).
- [13] M. Hashimoto, Y. Ishida, R. Yamamoto, and M. Doyama, Thermodynamic properties of coincidence boundaries in aluminum, *Acta Metal.* **29**, 617 (1981).
- [14] R. Najafabadi, D. J. Srolovitz, and R. LeSar, Thermodynamic and structural properties of [001] twist boundaries in gold, *J. Mater. Res.* **6**, 999 (1991).
- [15] A. Hairie, F. Hairie, B. Lebouvier, G. Nouet, E. Paumier, N. Ralantoson, and A. P. Sutton, Free energies of interfaces from quasi-harmonic theory: A critical appraisal, *Interface Sci.* **2**, 17 (1994).
- [16] D. J. Harris, G. W. Watson, and S. C. Parker, Atomistic simulation of the effect of temperature and pressure on the [001] symmetric tilt grain boundaries of MgO, *Philos. Mag. A* **74**, 407 (1996).
- [17] S. M. Files, Temperature dependence of grain boundary free energy and elastic constants, *Scripta Mater.* **62**, 231 (2010).
- [18] J. R. Morris, Z.-Y. Lu, D. M. Ring, J.-B. Xiang, K.-M. Ho, and C. Z. Wang, First-principles determination of the  $\Sigma = 13$  {510} symmetric tilt boundary structure in silicon and germanium, *Phys. Rev. B* **58**, 11241 (1998).
- [19] N. A. Benedek, A. L.-S. Chua, and C. Elsässer, Interatomic potentials for strontium titanate: An assessment of their transferability and comparison with density functional theory, *Phys. Rev. B* **78**, 064110 (2008).
- [20] G. Kresse and J. Hafner, *Ab initio* molecular dynamics for liquid metals, *Phys. Rev. B* **47**, 558 (1993).
- [21] G. Kresse and J. Hafner, *Ab initio* molecular-dynamics simulation of the liquid-metal-amorphous-semiconductor transition in germanium, *Phys. Rev. B* **49**, 14251 (1994).
- [22] G. Kresse and J. Furthmüller, Efficiency of ab-initio total energy calculations for metals and semiconductors using a plane-wave basis set, *Comput. Mater. Sci.* **6**, 15 (1996).
- [23] J. P. Perdew, K. Burke, and M. Ernzerhof, Generalized Gradient Approximation Made Simple, *Phys. Rev. Lett.* **77**, 3865 (1996).
- [24] P. E. Blöchl, Projector augmented-wave method, *Phys. Rev. B* **50**, 17953 (1994).
- [25] G. Kresse and D. Joubert, From ultrasoft pseudopotentials to the projector augmented-wave method, *Phys. Rev. B* **59**, 1758 (1999).
- [26] H. J. Monkhorst and J. D. Pack, Special points for Brillouin-zone integrals, *Phys. Rev. B* **13**, 5188 (1976).
- [27] M. Boiocchi, F. Caucia, M. Merli, D. Prella, and L. Ungaretti, Crystal-chemical reasons for the immiscibility of periclase and wüstite under lithospheric P, T conditions, *Eur. J. Mineral.* **13**, 871 (2001).
- [28] K. P. McKenna and A. L. Shluger, First-principles calculations of defects near a grain boundary in MgO, *Phys. Rev. B* **79**, 224116 (2009).
- [29] M. L. Kronberg and F. H. Wilson, Secondary recrystallization in copper, *JOM* **1**, 501 (1949).
- [30] V. Vitek, Intrinsic stacking faults in body-centered cubic, *Philos. Mag.* **18**, 773 (1968).
- [31] See Supplemental Material at <http://link.aps.org/supplemental/10.1103/PhysRevMaterials.4.026002> for a comparison between harmonic and quasiharmonic approximations for the  $\Sigma 5(310)/[001]$  and the most stable and metastable GB structures used for lattice dynamics calculations.
- [32] A. Togo and I. Tanaka, First principles phonon calculations in materials science, *Scr. Mater.* **108**, 1 (2015).
- [33] G. W. Watson, E. T. Kelsey, N. H. de Leeuw, J. Harris, and S. C. Parker, Atomistic simulation of dislocations, surface and interfaces in MgO, *J. Chem. Soc. Faraday Trans.* **92**, 433 (1992).
- [34] F. Landuzzi, L. Pasquini, S. Giusepponi, M. Celino, A. Montone, P. L. Palla, and F. Cleri, Molecular dynamics of ionic self-diffusion at an MgO grain boundary, *J. Mater. Sci.* **50**, 2502 (2015).
- [35] T. Yokoi and M. Yoshiya, Atomistic simulations of grain boundary transformation under high pressures in MgO, *Physica B Condens. Matter.* **532**, 2 (2018).
- [36] J. H. Harding, D. J. Harris, and S. C. Parker, Computer simulation of general grain boundaries in rocksalt oxides, *Phys. Rev. B* **60**, 2740 (1999).
- [37] A. K. Verma and B. B. Karki, First-principles simulations of MgO tilt grain boundary: Structure and vacancy formation at high pressure, *Am. Mineral.* **95**, 1035 (2010).

- [38] D. M. Saylor, A. Morawiec, and G. S. Rohrer, Distribution of grain boundaries in magnesia as function of five macroscopic parameters, *Acta Mater.* **51**, 3663 (2003).
- [39] F. Papillon, G. S. Rohrer, and P. Wynblatt, Effect of segregating impurities on the grain-boundary character distribution of magnesium oxide, *J. Am. Ceram. Soc.* **92**, 3044 (2009).
- [40] M. A. Tschopp and D. L. McDowell, Structures and energies of  $\Sigma 3$  asymmetric tilt grain boundaries in copper and aluminium, *Philos. Mag.* **87**, 3147 (2007).
- [41] M. A. Tschopp and D. L. McDowell, Asymmetric tilt grain boundary structure and energy in copper and aluminium, *Philos. Mag.* **87**, 3871 (2007).